

1 **Temporal Variability of Waves at the Proton Cyclotron Frequency Upstream**
2 **from Mars: Implications for Mars Distant Hydrogen Exosphere.**

3

4 C. Bertucci^{1,2*}, N. Romanelli¹, J.Y. Chaufray³, D. Gomez^{1,2}, C. Mazelle⁴, M. Delva⁵,
5 R. Modolo³, F. González-Galindo⁶, and D. A. Brain⁷.

6

7 1) Instituto de Astronomía y Física del Espacio, CONICET/UBA, Buenos Aires,
8 Argentina.

9 2) Departamento de Física, FCEN, Universidad de Buenos Aires, Argentina

10 3) LATMOS, Guyancourt, France

11 4) IRAP, Toulouse, France

12 5) IWF-ÖAW, Graz, Austria

13 6) Instituto de Astrofísica de Andalucía, Granada, Spain.

14 7) University of Colorado, USA.

15 * Corresponding author (cbertucci-at-iafe.uba.ar)

16

17 **Abstract**

18 We report on the temporal variability of the occurrence of waves at the local proton
19 cyclotron frequency upstream from the Martian bow shock from Mars Global
20 Surveyor observations during the first aerobraking and science phasing orbit periods.
21 Observations at high southern latitudes during minimum-to-mean solar activity show
22 that the wave occurrence rate is significantly higher around perihelion/southern
23 summer solstice and lower around the same hemisphere's spring and autumn
24 equinoxes. A similar trend is observed in the hydrogen (H) exospheric density profiles
25 over the Martian South Pole obtained from a model including UV thermospheric

26 heating effects. In spite of the complexity in the ion pick-up and plasma wave
27 generation and evolution processes, these results support the idea that variations in the
28 occurrence of waves could be used to study the temporal evolution of the distant
29 Martian H corona and its coupling with the thermosphere at altitudes currently
30 inaccessible to direct measurements.

31

32 **Keywords:**

33 Mars; Waves; Exosphere; Hydrogen; Thermosphere; Pick-up

34

35 **1. Introduction**

36 The absence of a significant intrinsic magnetic field at Mars (Acuña et al., 1998)
37 results in the direct interaction of the magnetized Solar Wind (SW) with the planet's
38 atmosphere. Mars interaction starts far beyond the bow shock, where exospheric
39 particles get ionized. Ionization processes add a small amount of energy to the
40 newborn ions with respect to their neutral precursors. As the latter are considered to
41 be approximately at rest with respect to the planet, the planetocentric velocities of
42 newborn ions are also assumed to be negligible. The newborn ion's initial motion in
43 the SW frame consists in a gyration (ring component) around the interplanetary
44 magnetic field (IMF) and a parallel motion (beam component) at the speed of its
45 neutral precursor. The speeds of the beam and ring components are: $V_{\parallel} = V_{\text{SW}} \cos(\alpha_{\text{VB}})$
46 and $V_{\perp} = V_{\text{SW}} \sin(\alpha_{\text{VB}})$ respectively, where α_{VB} , the IMF cone angle, is the
47 initial pitch angle of the newborn ion and V_{SW} is the velocity of the solar wind. The
48 newborn ion distribution function arising from the pick-up of a large number of
49 planetary ions is unstable to the growth of plasma low frequency waves (Wu and
50 Davidson, 1972). In particular, the occurrence of waves at the local cyclotron

51 frequency $\Omega_i = q_i B / m_i$ (B is the magnetic field strength, and q_i and m_i are the charge
52 and mass of the ion respectively) of a particular ion in the SC frame can be associated
53 with the occurrence of the exospheric pick-up of ions with a specific mass-per-charge
54 ratio. This represents a potentially useful diagnostic tool to detect ionized exospheric
55 particles. An extensive discussion on the way in which magnetic field wave
56 measurements in the SC frame can be associated with ion-ion instabilities arising
57 from the pick-up of exospheric ions can be found in Romanelli et al. (2013).

58 At Mars, Phobos-2 and Mars Global Surveyor (MGS) magnetometers detected
59 upstream waves at the local proton cyclotron frequency Ω_p (Russell, et al., 1990,
60 Brain et al., 2002; Mazelle et al., 2004; Wei and Russell, 2006; Romanelli et al.,
61 2013). All cases analyzed show a left-hand polarization in the SC frame, and a quasi-
62 parallel propagation with respect to the IMF. Romanelli et al. (2013) analyzed the
63 properties of upstream waves at Ω_p from a set of 372 MGS orbits from 27 March 1998
64 to 24 September 1998, during the science phasing orbits (SPO) phase. They revealed
65 that the occurrence of waves at Ω_p strongly dropped between SPO1 (62% of the
66 upstream observation time) and SPO2 (8%) sub-phases. They also noted no
67 significant difference in the directional properties of the IMF, α_{VB} , or the IMF's
68 convective electric field between the two sub-phases, suggesting that the reduction in
69 wave occurrence could be due to temporal changes in the density of pick-up protons.

70 Theoretical and observational studies have confirmed that the source of the pick-up
71 ions responsible for the occurrence of waves at Ω_p at Mars is its hydrogen (H)
72 exosphere via ionization processes such as photoionization and charge exchange
73 (Barabash and Lundin, 2006; Dennerl et al., 2006). As in the case of Venus, the
74 Martian (H) corona has been hypothesized to contain a hot and a relatively cooler
75 thermal population (see, e.g., Johnson et al., 2008). A recent work by Chaufray et al,

76 (2008) based on Mars Express SPICAM observations suggests the presence of hot (T
77 > 500 K) and cold ($T \sim 200$ K) populations. However, the inferred hot H densities are
78 not supported by theory and the two-population model is still poorly constrained by
79 observations and model errors. Other works find inconclusive evidence for a two-
80 population model (Feldman et al., 2011) and provide single profiles.

81 So far, only models and indirect observations can predict the structure of the
82 exosphere at altitudes higher than a few scale heights above the exobase. Most models
83 use a Chamberlain (1963) approach based on isothermal equilibrium. The vertical
84 profile of the exospheric number density is an exponential whose scale height is a
85 function of the exobase temperature and density, provided by models or observations.
86 Long term (timescales larger than diurnal) variations in the modeled exospheric
87 densities come mainly from UV heating of the thermosphere. As a result, solar cycle,
88 annual and seasonal influences are expected. Simulations including a self-consistent
89 calculation of the global ion production (Modolo et al., 2005) show that H escape is
90 strongly dependent on the EUV flux through its influence on exospheric densities.

91 In this work, we study the temporal variability of the occurrence of upstream waves at
92 Ω_p at Mars based on MGS MAG observations during the first Aerobraking (AB1) and
93 SPO phases and we propose an explanation for the observed trends based on the
94 behavior of Mars distant H exosphere. Then, we discuss the implications of these
95 results in the understanding of Mars H corona and its interaction with the solar wind.

96

97 **2. Observations**

98 MGS MAG is a dual fluxgate magnetometer that provides fast (up to 32 Hz), wide
99 range (± 4 , ± 65335 nT) magnetic field measurements with an uncertainty of ± 1 nT due
100 to spacecraft fields (Acuña et al., 2001). Typical values for the proton cyclotron

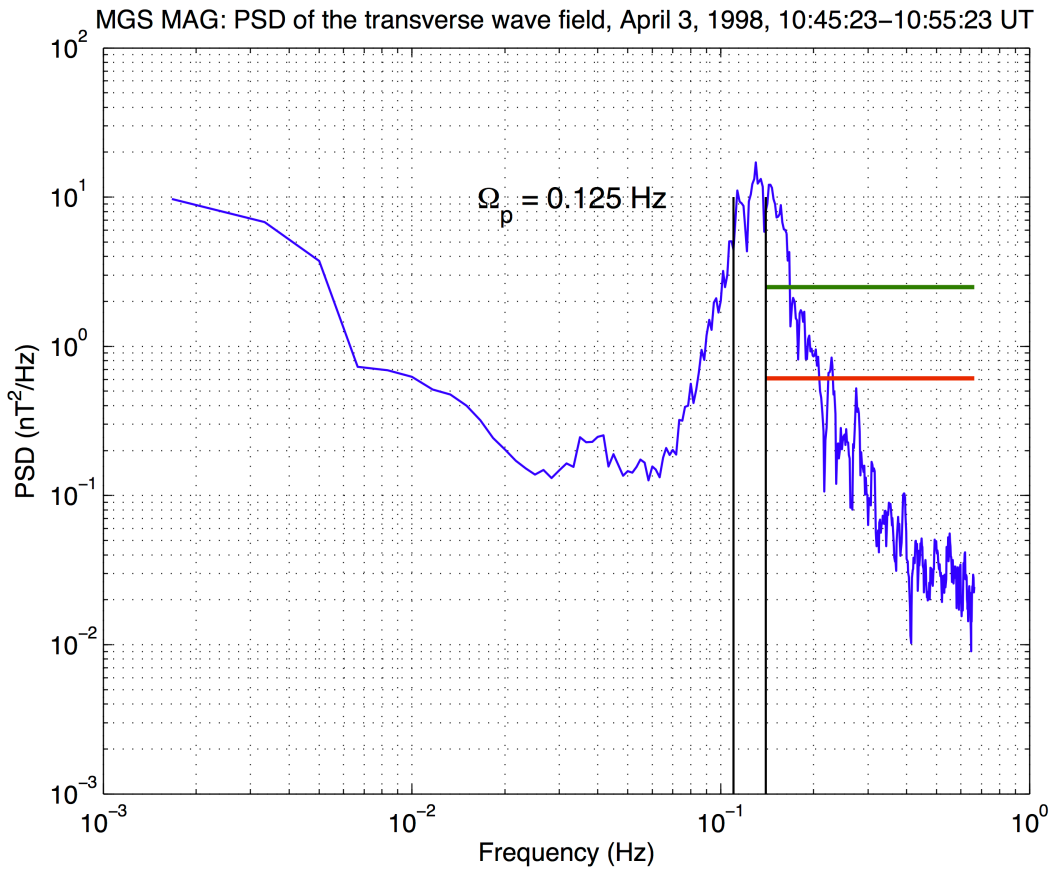
101 frequency at Mars orbit (~ 0.05 Hz) justify the use of low-resolution MAG data
102 (0.167 - 1.33 Hz) for which additional calibration is available.

103 After Mars orbit insertion/capture (MOI) on September 11, 1998, MGS was placed in
104 highly elliptical orbits with apoapses approximately located over the planet's South
105 Pole. The evolution of MGS orbital period from MOI through the entire pre-mapping
106 phase is described in Figure 6 from Albee et al. (2001). The aerobraking applied
107 between MOI and April 1998 reduced the orbital period from 48 to 12 h; this phase is
108 known as AB1. SPO came in after AB1 and ended in November 1998, when a second
109 aerobraking (AB2) phase began. SPO orbits were 12-hour long and local times
110 monotonically varying between noon and 4AM. During AB1 and SPO, the southern
111 latitudes of the apoapses remained high.

112 The upstream segments of every AB1 and SPO orbit were examined in the search for
113 waves at Ω_p . Since these waves propagate almost parallel to the IMF (Romanelli et
114 al., 2013), the criterion used to identify them was based on the Fourier power spectral
115 density (PSD) of the transverse wave components with respect to the IMF ($\delta\mathbf{B}_\perp$). The
116 PSD of $\delta\mathbf{B}_\perp$ is the norm of a vector whose components are the power spectral densities
117 the components of $\delta\mathbf{B}_\perp$. Its value is estimated over sliding 10-minute intervals with an
118 overlap of 1 minute. Upstream portions are identified using the points where MGS
119 trajectory crosses Vignes et al (2000) bow shock fit, assuming an error of 10 minutes
120 on the upstream side along the spacecraft trajectory.

121 We define that waves at Ω_p are detected when the average PSD within the frequency
122 band $\Omega_p \pm 0.015$ Hz (0.015 Hz being the error in Ω_p associated with MAG's
123 uncertainty) is larger than the average PSD for frequencies $\omega > \Omega_p + 0.015$ Hz, plus
124 its standard deviation (STD), multiplied by a constant $k > 1$. If f_N is the Nyquist

125 frequency (0.167 and 0.667 Hz for the two low frequency sampling rates available),
 126 this is: $\langle PSD(\omega) \rangle_{\Omega_p-0.015Hz}^{\Omega_p+0.015Hz} > k \{ \langle PSD(\omega) \rangle_{\Omega_p+0.015Hz}^{f_N} + STD\{PSD(\omega)\}_{\Omega_p+0.015Hz}^{f_N} \}$.
 127 The value of k is obtained by inspecting several orbits with and without a clear
 128 spectral line at Ω_p . A value of $k = 2.5$ was found to be acceptable as all selected orbits
 129 show signatures at Ω_p , and their number is adequate for statistical purposes. Similar
 130 criteria have been applied on Venus Express magnetometer measurements (Delva et
 131 al., 2011, and references therein).



133 *Figure 1. PSD of $\delta\mathbf{B}_\perp$ for 10:45:23–10:55:23 on April 3, 1998 for a case of positive detection of waves*
 134 *at Ω_p . Black lines indicate the frequency range corresponding to the error in the estimate of Ω_p due to*
 135 *spacecraft fields (Acuña et al., 2001). The average power density for frequencies higher than the upper*
 136 *limit of the interval is indicated in red. The green line shows that average plus the standard deviation.*
 137 *The latter value is 3.92 times smaller than the power in the interval around Ω_p .*

138

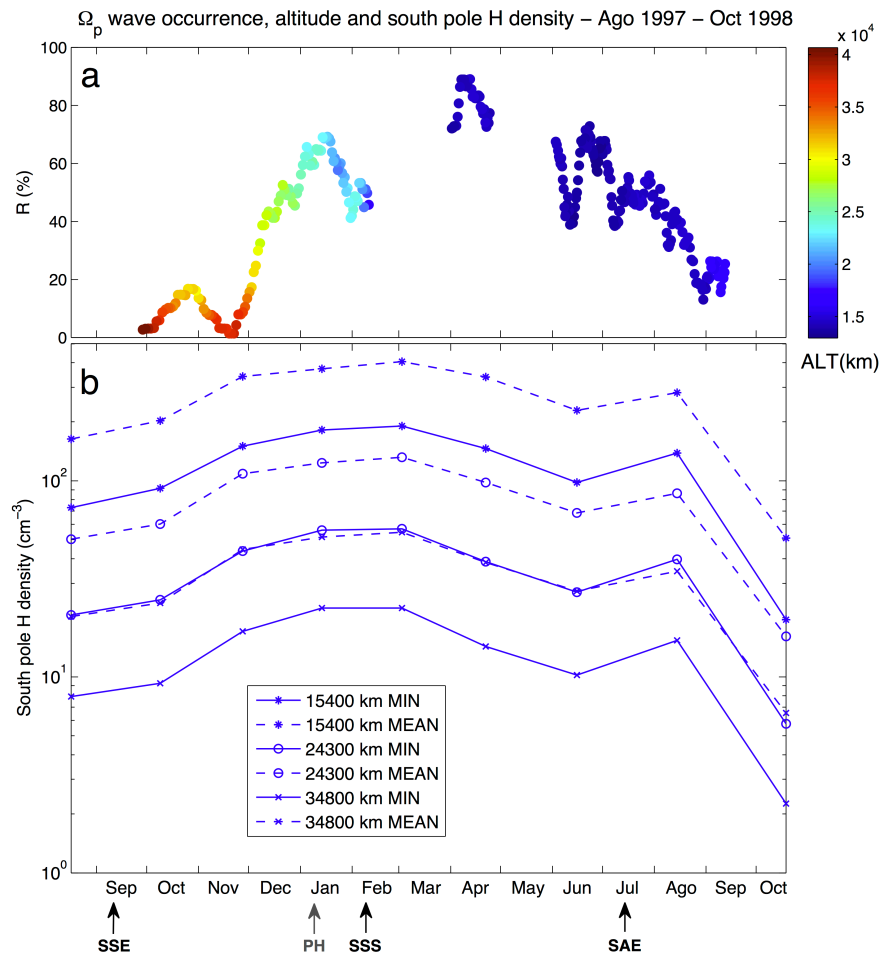
139 Figure 1 shows an example of a positive detection of waves at Ω_p . The plot shows the
140 PSD of $\delta\mathbf{B}_\perp$ as a function of frequency ω for the interval 10:45:23-10:55:23 on April
141 3, 1998. The spectrum shows a peak at $\Omega_p = 0.125$ Hz in the SC frame. The power
142 contained in the 0.105 - 0.135 Hz band (black lines) is higher than the average power
143 contained at higher frequencies (red line), plus that power's STD (green line).

144 For statistical purposes, a wave occurrence rate for each orbit was estimated as the
145 number of intervals meeting the criterion above, divided by the total number of
146 intervals in the upstream portion of the orbit. The occurrence rates are then averaged
147 every 15 orbits with a 14-orbit overlap, regardless of the orbit period. The averaged
148 occurrence rate is hereafter referred to as R.

149

150 **3. Results and Discussion**

151 Figure 2a shows the evolution of R between September 14, 1997 and September 17,
152 1998 (AB1, and SPO). Data gaps corresponding to the AB1-SPO1 transition
153 (February 20 - March 26, 1998), and solar conjunction hiatus (April 30 - May 26,
154 1998) are apparent. The occurrence rate exhibits an increase at the very beginning of
155 the mission -around the southern spring equinox (September 12, 1997). R reaches a
156 local maximum of 19% around October 27, 1997 and then goes back to near zero
157 around day November 16, 1997. After that, R increases again, and reaches 50% by the
158 end of the year, and a maximum at 68 % a few days after Mars perihelion (January 7,
159 1998). After January 12, the wave abundance falls again, but this time values remain
160 above 40% before the first data gap. The highest values around 89% are clustered
161 around April 1998, during southern summer. After solar conjunction, a more gradual
162 decrease is observed, with values around 20% during early southern autumn.
163 Occurrence rates are consistent with the map by Brain et al. (2002).



164

165 *Figure 2a: Occurrence of waves at Ω_p from Sep. 1997 through Sep. 1998 averaged every 15 MGS*166 *orbits. Points are color-coded according to the upstream average altitude (see text for details). Figure*167 *2b: Modeled exospheric H density above Mars South Pole at 15400, 24300 and 34800 km altitude for*168 *minimum and mean solar activity from Aug. 1997 to Oct. 1998. Dates for Mars perihelion (PH,*169 *January 7, 1998), southern hemisphere spring equinox (SSE, 12 September 1997), southern*170 *hemisphere summer solstice (SSS, February 6, 1998), and southern hemisphere autumn equinox (SAE,*171 *July 14, 1998) are indicated.*

172

173 *The changes in R can be better understood if the average altitudes of the upstream*174 *orbit portions are considered. Mean altitudes are higher during AB1 (~30000 km),*175 *where fewer wave events are observed. In particular an anti-correlation between R*

176 and the average altitude is observed until January 1998. During SPO, average
177 altitudes are around 13600 km, suggesting a weaker influence of radial distance on R.
178 Figure 2a suggests a temporal dependence in the abundance of upstream waves at Ω_p .
179 The hypothesis that any variability in the wave occurrence at a given location is
180 attributed to temporal effects is supported by the strong difference in wave abundance
181 for orbits with similar geometry, and the absence of a manifest influence upon the
182 convective electric field or the IMF direction (Romanelli et al., 2013). In what
183 follows, changes in the efficiency of the wave generation mechanism, the properties
184 of the solar wind, the efficiency of the ionization mechanisms and/or the local
185 exospheric H density are discussed in the context of MGS observations.

186

187 *3.1 Wave generation and evolution*

188 A central question is how representative the presence of waves at Ω_p is for the local
189 neutral density. Cowee et al. (2012) suggest that the increase in the amplitude of
190 waves at Ω_p is due to the increase in the local pick-up ion density and the cumulative
191 ion production upstream of the observation point. As exospheric densities increase,
192 increases in both the local and cumulative ion productions are expected. Accordingly,
193 higher occurrence rates will be expected at Ω_p as long as nonlinear effects do not
194 degrade the wave spectra below the detection threshold. According to Cowee et al.,
195 (2012) the observed waves would be below nonlinear saturation.

196 Another aspect to consider is that the wavelength for maximum linear growth rates at
197 least for the ion-ion right hand mode is of the order of a Martian radius (Bertucci,
198 2003), setting a limit on the spatial resolution in the use of waves as indicators of
199 exospheric densities. To avoid this limitation, comparisons between the spatial

200 distributions of waves and exospheric densities are restricted to length scales greater
201 than a planetary radius.

202

203 *3.2 Changes in Solar wind parameters and ionization rates*

204 Self-consistent hybrid simulations (Modolo et al., 2005) suggest that charge exchange
205 is the main source of escaping protons and that the escape rate of these protons is four
206 times higher during solar minimum with respect to solar maximum due to the
207 expansion of the neutral H corona. Although MGS measurements are not able to
208 characterize the photoionization and charge exchange rates, the solar activity during
209 the pre-mapping phase was typical of a minimum, suggesting that both ionization
210 rates would not have experienced major alterations. In agreement with this view,
211 recent works addressing the generation of the same type of waves (Cowee et al.,
212 2012) assume constant ionization rates.

213 Transient solar wind disturbances such as ICMEs have been proven to alter
214 significantly the Martian plasma environment (Crider et al., 2005). Once again, the
215 expected low solar activity, the absence of drastic short-term (a few days long)
216 changes in the wave abundance, and the fact that from September 1997 to September
217 1998 the solar F10.7 flux at Mars did not vary significantly ($107.90 \pm 18.59 \text{ cm}^{-2} \text{ s}^{-1}$)
218 suggest that such events might not be the cause of the long term variability of R.

219

220 *3.3 Changes in the extent of the distant Martian hydrogen corona*

221 Figure 2b shows values of H exospheric density above the Martian South Pole at
222 15400, 24300 and 34800 km altitude for solar mean and minimum activity conditions
223 between August 1997 and October 1998. H densities are provided by a 3D exospheric
224 model (Chaufray et al. 2012), which incorporates non-uniform densities and

225 temperatures at the exobase from a 3D LMD-GCM model (Gonzalez-Galindo et al.
226 2009). Values initially given as a function of solar longitude are then converted to
227 time using MGS ephemeris. Three basic properties are immediately evident. First,
228 densities fall by one order of magnitude between 15400 and 34800 km for each solar
229 activity scenario. Second, H densities increase with solar activity, which reveals the
230 UV control of the thermosphere. Third, the influence of solar declination and
231 heliocentric distance is manifested in density curves displaying maxima slightly after
232 Mars perihelion and southern summer solstice (February 6, 1998), and lower values
233 during spring and autumn. H densities are not symmetric around their maxima. This is
234 probably due to heliocentric distance effects (aphelia occurred on January 29, 1997,
235 and December 16, 1998, respectively).

236 Although the wave growth rate depends on several factors, the observed variability in
237 R could be explained from MGS orbital geometry and the annual and seasonal
238 changes in the H exospheric profile predicted by models. Early in AB1, MGS
239 explored, on average, regions with altitudes around the 34800 km altitude level during
240 solar minimum. The low H densities at that altitude for solar minimum (around 10 cm^{-3})
241 ³) could be responsible for the low wave occurrence rates observed. Furthermore, the
242 increase in R around the end of October 1997 is consistent with MGS exploring lower
243 altitudes, where higher H densities ($\sim 20 \text{ cm}^{-3}$) and wave amplitudes (Romanelli et al.,
244 2013) are expected. As AB1 progresses, the increase in the wave occurrence could be
245 a result of both the decrease in the average altitude of the observations and the
246 increase in the local H density as southern summer approached. The peak in
247 occurrence observed in mid January 1998 is followed by a short $\sim 20\%$ drop which
248 cannot be explained, as predicted H densities remain high and average orbital altitude
249 continues to decrease.

250 The rather constant average altitudes during SPO allow a direct comparison of the
251 wave abundance and H density curves the lowest altitude level. Apart from the data
252 gaps, these curves display similar trends, as the southern hemisphere gradually
253 transits towards the autumn equinox (July 14, 1998). The gradual decrease in R could
254 be then due to the change in exospheric densities with solar activity. Finally, in mid
255 September, the wave abundance is around 20 % and local predicted densities are
256 closer to the values expected in mean solar activity conditions ($\sim 20 \text{ cm}^{-3}$).

257 This comparison provides a possible explanation to the temporal variability in the
258 occurrence of waves at Ω_p , based on the expansion and contraction of the Martian H
259 exosphere due to annual and seasonal components in the solar UV heating of the
260 thermosphere. If this is confirmed, the temporal variability in the occurrence of waves
261 at Ω_p could be used to study the coupling of the thermosphere with the exosphere of
262 Mars (Bougher et al., 1999), where direct observations are unavailable. In particular,
263 wave observations coincide with the occurrence of dust storms of varied intensity
264 (Keating, et al., 1998; Clancy et al., 2000) with known effects on the Martian
265 thermosphere.

266 The influence of the exosphere in the Martian solar wind interaction has also been
267 suggested to be responsible for other plasma structures such as the magnetic pileup
268 boundary (MPB, see, e.g., Crider et al., 2000). A study based on MGS MAG/ER data
269 during the mapping phase revealed that the altitude of the northern MPB (i.e., far
270 from the influence of crustal fields) is sensitive to Martian seasons (Brain et al.,
271 2005). The question whether this behavior is related to the hypotheses presented here
272 or not is beyond the scope of this work. Nevertheless, all these results suggest that in
273 addition to the solar cycle, the annual and seasonal variability in the UV irradiance

274 could be a potentially important component of the temporal evolution of the Martian
275 plasma environment.

276

277 **4. Conclusions**

278 The pick-up of exospheric ions, and the subsequent growth and evolution of plasma
279 waves via microscopic plasma interactions are complex physical processes. By virtue
280 of a particular property of waves propagating along the IMF and originating from
281 exospheric ion pick-up, the analysis of the occurrence of upstream transverse
282 fluctuations at Ω_p at high southern latitudes shows that the abundance of such waves
283 varies with time. This temporal variability is found to display similar trends as those
284 of the densities of exospheric H obtained from models, which take the effect of
285 thermospheric heating by solar UV radiation into account. The underlying assumption
286 is that wave generation mainly depends on the H local density and that ionization
287 rates remain constant. This approach follows previous works, which suggest that the
288 increase in the ion production is due to changes in the exospheric densities.

289 Future studies based on improved exospheric models and more comprehensive
290 measurements (such as those to be carried out by the MAVEN mission) will help to
291 confirm or discard the proposed interpretation. In particular, the effects of the vertical
292 transfer of energy and momentum at different timescales, including the role of global
293 atmospheric events such as dust storms should be investigated.

294

295 **References**

296 Acuña, M., et al., Magnetic field and plasma observations at Mars: initial results of
297 the Mars Global Surveyor Mission, *Science*, 279, 1676–1680, 1998.

- 298 Acuña, M.H., et al., Magnetic field of Mars: Summary of results from the aerobraking
299 and mapping orbits, *J. of Geophys. Res.*, 106, E10, 23403-23418, 2001.
- 300 Albee, A. L., et al. Overview of the Mars Global Surveyor mission. *J. Geophys. Res.*,
301 106(E10), 23,291–23,316, (2001).
- 302 Barabash, S., Lundin, R., ASPERA-3 on Mars Express, *Icarus*, 182, 2, 301-307, 2006.
- 303 Bertucci, C., PhD Thesis, Université Paul Sabatier, France, 2003.
- 304 Bougher, S., et al., Mars Global Surveyor aerobraking: atmospheric trends and model
305 interpretation, *Adv. Space Res.*, 23, 11, 1887-1897, 1999.
- 306 Brain, D.A., et al., Observations of low-frequency electromagnetic plasma waves
307 upstream from the Martian shock, *J. Geophys. Res.*, 107 (A6), 1076, 2002.
- 308 Brain, D.A, et al., Variability of the altitude of the Martian sheath, *Geophys. Res.*
309 *Lett.*, 32, .18, CiteID L18203, 2005.
- 310 Chaufray, J.Y., et al., Observation of the hydrogen corona with SPICAM on Mars
311 Express, *Icarus* 195 (2), 598–613, 2008.
- 312 Chaufray J.-Y., et al., Current status on Mars exospheric studies, 39th COSPAR
313 Scientific Assembly, Mysore : India (2012) - hal-00740343
- 314 Chamberlain, J. W., Planetary coronae and atmospheric evaporation, *Planet. Space*
315 *Sci.*, 11, 8, 901–960, 1963.
- 316 Clancy, R.T., et al., An intercomparison of ground-based millimeter, MGS TES, and
317 Viking atmospheric temperature measurements: Seasonal and interannual variability
318 of temperatures and dust loading in the global Mars atmosphere, *J. Geophys. Res.*,
319 105, E4, 9553-9571, 2000.
- 320 Cowee, M.M., et al., Pickup ions and ion cyclotron wave amplitudes upstream of
321 Mars: first results from the 1D hybrid simulation. *Geophys. Res. Lett.*, 39, L08104,
322 doi: 10.1029/ 2012GL051313, 2012.

- 323 Crider, D. H., et al., Evidence of electron impact ionization in the magnetic pileup
324 boundary of Mars. *Geophys. Res. Lett.*, 27(1), 45–48, 2000.
- 325 Crider, D. H., et al., Mars Global Surveyor observations of the Halloween 2003 solar
326 superstorm's encounter with Mars, *J. Geophys. Res.*, 110, A09S21,
327 doi:10.1029/2004JA010881, 2005.
- 328 Delva, M., et al., Upstream Ion Cyclotron Waves at Venus and Mars, *Space Sci. Rev.*,
329 Vol. 162, Issue 1-4, pp. 5-24, 2011.
- 330 Dennerl, K., et al., First observation of Mars with XMM–Newton. High resolution X-
331 ray spectroscopy with RGS, *Astron. Astrophys.*, 451, 709–722, 2006.
- 332 Feldman, P., et al., Rosetta-Alice observations of exospheric hydrogen and oxygen on
333 Mars, *Icarus*, Vol. 214, Issue 2, p. 394-399, 2011.
- 334 Gary, S.P., Theory of space plasma microinstabilities. In: *Cambridge Atmospheric
335 and Space Series*. Cambridge University Press, 1993.
- 336 Gonzalez-Galindo, F., et al., A ground-to-exosphere Martian circulation model: 1
337 Seasonal, diurnal and solar cycle variation of thermospheric temperatures, *J. Geophys.
338 Res*, 114, E04001, doi:10.1029/2008JE003246, 2009.
- 339 Johnson, R.E., et al., Exospheres and Atmospheric Escape, *Space Sci. Rev.*, 139: 355–
340 397 DOI 10.1007/s11214-008-9415-3, 2008.
- 341 Keating, G.M., et al., The Structure of the Upper Atmosphere of Mars: In Situ
342 Accelerometer Measurements from Mars Global Surveyor, *Science*, 279, 5357, p.
343 1672, 1998.
- 344 Mazelle, C., et al., Bow shock and upstream phenomena at Mars, *Space Sci. Rev.*,
345 111, 115–181, 2004.
- 346 Modolo, R., et al., Influence of the solar EUV flux on the Martian plasma
347 environment, *Ann. Geophys.*, vol. 23, Issue 2, pp.433-444, 2005.

348 Romanelli, N., et al., Proton cyclotron waves upstream from Mars: Observations from
349 Mars Global Surveyor, *Planet. Space Sci.*, 76, 1-9, 2013.

350 Russell, C.T., et al., Upstream waves at Mars—PHOBOS observations. *Geophys.*
351 *Res. Lett.*, 17 (6), 897–900, 1990.

352 Vignes, D., et al., The Solar Wind interaction with Mars: locations and shapes of the
353 Bow Shock and the Magnetic Pile-up Boundary from the observations of the
354 MAG/ER experiment onboard Mars Global Surveyor. *Geophys. Res. Lett.*, 27, 1, 49-
355 52, 2000.

356 Wei, H., Russell, C.T., Proton cyclotron waves at Mars: exosphere structure and
357 evidence for a fast neutral disk, *J. Geophys. Res.*, 33, L23103, 2006.

358 Wu, C. S., Davidson, R., C., Electromagnetic instabilities produced by neutral-particle
359 ionization in interplanetary space, *J. Geophys. Res.*, 77, 28, p. 5399, 1972.

360

361 **Acknowledgements**

362 This work was done in conjunction with the International Space Science Institute
363 (ISSI) International Team on Comparative Induced Magnetospheres. FGG is funded
364 by a CSIC JAE-Doc contract co-financed by the European Social Fund.

365